















High-spin level structure of ^{209}Rn

Sneha Das ^{1,2}, S. Bhattacharyya ^{1,2,*}, Soumik Bhattacharya ¹, S. Chakraborty ¹, Sakshi Shukla ³, Praveen C. Srivastava ³, R. Banik ^{1,†}, S. Nandi ^{1,‡}, G. Mukherjee ^{1,2}, Indu Bala,⁴ S. S. Bhattacharjee,⁴ S. Das Gupta,⁵ A. Dhal,^{1,§} Debasish Mondal ¹, S. Muralithar,⁴ R. Raut ⁶, A. Sharma ⁷, R. P. Singh ⁴ and V. Srivastava ^{4,||}

¹Variable Energy Cyclotron Centre, Kolkata - 700064, India

²Homi Bhabha National Institute, Anushaktinagar, Mumbai - 400094, India


³Department of Physics, Indian Institute of Technology Roorkee, Roorkee - 247667, India

⁴Inter-University Accelerator Centre, New Delhi - 110067, India

⁵Department of Physics, Victoria Institution (College), Kolkata - 700009, India

⁶UGC-DAE Consortium for Scientific Research, Kolkata Centre, Kolkata - 700107, India

⁷Department of Physics, Himachal Pradesh University, Shimla - 171005, India

 (Received 4 August 2023; revised 1 September 2023; accepted 7 December 2023; published 23 January 2024)

The excited states of ^{209}Rn ($Z = 86$, $N = 123$) have been populated by the heavy-ion induced fusion evaporation reaction $^{198}\text{Pt}(^{16}\text{O}, 5n)^{209}\text{Rn}$ at a beam energy of 102 MeV. The de-excited γ rays were detected with the Compton suppressed clover HPGe detectors of the Indian National Gamma Array (INGA) set-up. The high spin spectroscopic study of ^{209}Rn has been carried out up to an excitation energy of 7.9 MeV and spin $(55/2)\hbar$. Spin-parity assignments of the excited levels have been determined and are confirmed on the basis of the ratio of directional correlation and polarization asymmetry measurement. The possible presence of new isomeric states has been observed and the half-lives have been estimated. A negative parity sequence of $M1$ transitions has been observed which exhibits the property of magnetic rotation and is interpreted in the framework of semiclassical model calculation. The large basis shell-model calculation has been performed for all the nuclear levels and is found to be in well agreement with the experimental results.

DOI: [10.1103/PhysRevC.109.014322](https://doi.org/10.1103/PhysRevC.109.014322)

I. INTRODUCTION

The nuclei in the vicinity of the doubly magic shell closure of ^{208}Pb have been the topic of significant physics interest in the recent years. These nuclei exhibit a variety of nuclear structural phenomena, such as, shears band, neutron core excitation across $N = 126$ shell closure, and presence of several short-lived and long-lived isomers. With few proton particles above $Z = 82$ and few neutron holes in the $N = 126$ shell closure, the nuclear structure in these nuclei are mainly dominated by the single particle excitations. As the number of the valence nucleons are increased, the single particle configurations evolve towards the mixture of multinucleon configurations. Hence, the nuclei in this region provide a fertile ground to test the validity of the large basis shell-model calculations. Moreover, several shell-model calculations have been performed in this near Pb region by considering ^{208}Pb

as a stable core [1,2]. Further, the presence of the large spin differences between the close lying high- j neutron and proton orbitals give rise to several high-spin isomers in this region [3]. The $13/2^+$ isomeric state has been observed to be present systematically for all odd- A isotopes of the nuclei above $Z = 82$ [4]. The study of these isomeric states in this region provides further understanding in level structure of these nuclei.

The occupation of the high- j orbitals, e.g., $\pi h_{9/2}$, $\pi i_{13/2}$, $\nu i_{13/2}$, etc., by the valence proton particles and the neutron holes gives rise to the magnetic rotation (MR) band in this region. In this case, the higher spin states are mainly generated by the closing of the two blades of shears formed by the aligned proton and neutron angular momentum vectors. The rotational band resulting from this mechanism possesses increasing $B(M1)/B(E2)$ ratio, and decreasing $B(M1)$ value with increasing rotational frequency. While the presence of the MR band is a very common phenomenon around the neutron-deficient Pb region [5–7], the observation of the MR band [8–11] in the above Pb region ($Z = 82$) around $N = 126$ neutron shell closure is rare due to insufficient experimental data at the high spin. The presence of the MR band in this region has already been reported for $^{203,204}\text{At}$ ($Z = 85$) [12,13], ^{202}Bi ($Z = 83$) [14], $^{201,202}\text{Pb}$ ($Z = 82$) [15], and ^{206}Fr ($Z = 87$) [16]. For, Rn ($Z = 86$) isotopes, only the high spin spectroscopic study of ^{205}Rn indicates the presence of a MR band, based on the observation of a cascade of magnetic

*sarmi@vecc.gov.in

[†]Present address: Institute of Engineering and Management, Kolkata - 700091, India.

[‡]Present address: Subatech (IMT Atlantique, CNRS/IN2P3, Nantes Universite), 4 rue Alfred Kastler, 44307 Nantes cedex 3, France.

[§]Present address: Extreme Light Infrastructure - Nuclear Physics, Măgurele 077126, Romania.

^{||}Present address: Amity University, Patna - 801503, India.

dipole transitions [17]. For other odd- A Rn ($Z = 86$) isotopes, around $N = 126$ shell closure, e.g., ^{207}Rn and ^{211}Rn , the MR band has not been observed so far [18,19].

The existence of the ground state and the two lower spin states of ^{209}Rn were first proposed by Raich *et al.* [20] from the α decay of ^{213}Ra . Further, the other studies from decay spectroscopy of ^{209}Fr [21] and ^{213}Ra [22] also established the ground state, other low-lying spin states, and the γ ray transitions corresponding to these states. The first high spin spectroscopic study of ^{209}Rn by heavy-ion induced reaction was carried out by Poletti *et al.* [23]. The de-excited γ rays were detected using one Compton-suppressed and two unsuppressed Ge(Li) detectors along with a Si(Li) detector and a liquid scintillator detector. However, the placement and the spin-parity assignment of the levels above the $21/2^+$ isomeric state were uncertain. Moreover, the connections between several sequence of states at the higher spins were indicated from the coincidence relationships but the connecting transitions could not be observed. Therefore, a comprehensive spectroscopic study of ^{209}Rn with the large array of high resolution and high efficiency γ -ray detector set-up is required to explore the high-spin structure of ^{209}Rn .

In the present paper, the level structure of ^{209}Rn has been reported with the placement of 26 new transitions. The possible presence of new high-spin isomeric states has been indicated and the half-lives have been estimated. The single particle excited states and the half-life of the isomeric state has been well reproduced from the shell-model calculation. The presence of a new negative parity sequence of $M1$ transitions has been observed in ^{209}Rn and it has been interpreted as MR band under the framework of semiclassical model calculation.

II. EXPERIMENTAL DETAILS

The high spin states of ^{209}Rn are populated in the fusion evaporation reaction $^{198}\text{Pt}(^{16}\text{O}, 5n)$ at 102 MeV beam energy from the Pelletron Accelerator, IUAC, New Delhi [24]. The target is 99% isotopically enriched self-supporting foil of ^{198}Pt with 9.3 mg/cm² thickness. The de-exciting γ rays are detected using the Indian National Gamma Array (INGA) setup [25], consisted of 18 Compton suppressed clover HPGe detectors. The detectors have been arranged with respect to the beam direction as: Four detectors each at 148° and 123°, six detectors at 90°, two detectors each at 57° and 32°.

The list-mode data have been acquired in singles and coincidence mode using the analog data acquisition system CANDLE [26]. Offline data analysis was carried out using LAMPS [27], INGASORT [28], and RADWARE [29] software packages.

III. DATA ANALYSIS PROCEDURE

To study the coincidence relationship between the γ rays, the γ - γ symmetric matrix and γ - γ - γ cube were generated. For the assignment of spin and parity of excited energy levels, two asymmetric matrices were generated. To determine the ratio of directional correlation from the oriented states (R_{DCO}), a matrix has been generated by putting the data from 90° (θ_1) along one axis and that from 148° (θ_2) at another axis, using

the relation [30]

$$R_{\text{DCO}} = \frac{I_{\gamma_1} \text{ at } \theta_1, \text{ gated by } \gamma_2 \text{ at } \theta_2}{I_{\gamma_1} \text{ at } \theta_2, \text{ gated by } \gamma_2 \text{ at } \theta_1}. \quad (1)$$

For the present work, the value of R_{DCO} was found to be ≈ 0.9 – 1.0 (1.5 – 1.6) for pure stretched quadrupole transitions and ≈ 0.5 – 0.6 (1.0 – 1.1) for dipole transitions with a pure quadrupole (dipole) gating transition. The R_{DCO} values were found to be varied from 0.7 to 0.8 at the gates of pure quadrupoles for some mixed dipole transitions (depending on the mixing ratios) and for some pure dipole transitions decaying from the isomeric states.

Clover detectors can serve as Compton polarimeter because of its special geometry which can be used to determine the electromagnetic nature of the γ rays [31]. For the measurement of polarization asymmetry of the decaying γ rays, two asymmetric matrices were constructed from the Compton-scattered events of 90° detectors corresponding to the parallel and perpendicular events with respect to the reaction plane. The polarization asymmetry is defined as

$$\Delta_{\text{asym}} = \frac{a(E_\gamma)N_\perp - N_\parallel}{a(E_\gamma)N_\perp + N_\parallel}, \quad (2)$$

where N_\perp (N_\parallel) are the number of Compton-scattered photons of a γ ray in perpendicular (parallel) direction with respect to the reaction plane, and $a(E_\gamma)$ is the correction factor, which takes into account the asymmetry in the response of the detector array. The polarization asymmetry should be zero for a radioactive source, therefore $a(E_\gamma)$ is defined as [32]

$$a(E_\gamma) = \frac{N_\parallel(\text{unpolarized})}{N_\perp(\text{unpolarized})}. \quad (3)$$

In the present work, the decay transitions from a ^{152}Eu standard radioactive source have been used to extract the value of $a(E_\gamma)$. The variation of $a(E_\gamma)$ as a function of γ -ray energy (E_γ) has been fitted, using the equation $a(E_\gamma) = a_0 + a_1 E_\gamma$. The values of the coefficients are obtained as $a_0 = 0.964$ and $a_1 = 8.192 \times 10^{-6}$. The positive and the negative values of the Δ_{asym} corresponds to the electric and magnetic nature of the transitions, respectively.

In order to study the presence of isomers, several γ - γ symmetric matrices were generated by gating at the different coincident time windows of the total aligned Time to Amplitude Converter (TAC). The coincident time window was varied from 10 ns to 200 ns in the interval of 10 ns. The observed intensity of the γ rays above the isomer, at the gate of the transitions below the isomer, is related with the coincidence-time window by the following formula [33]:

$$N_t = N_0 \left(1 - A e^{-\frac{\ln 2}{T_{1/2}} \Delta t} \right), \quad (4)$$

where N_0 and N_t are the counts initially and at time t , respectively, $T_{1/2}$ = half-life of the isomeric state, Δt is the coincidence time window, A is used as a free fitting parameter.

IV. RESULTS

The level scheme of ^{209}Rn as obtained from the present work using coincidence relationships of the observed γ rays is

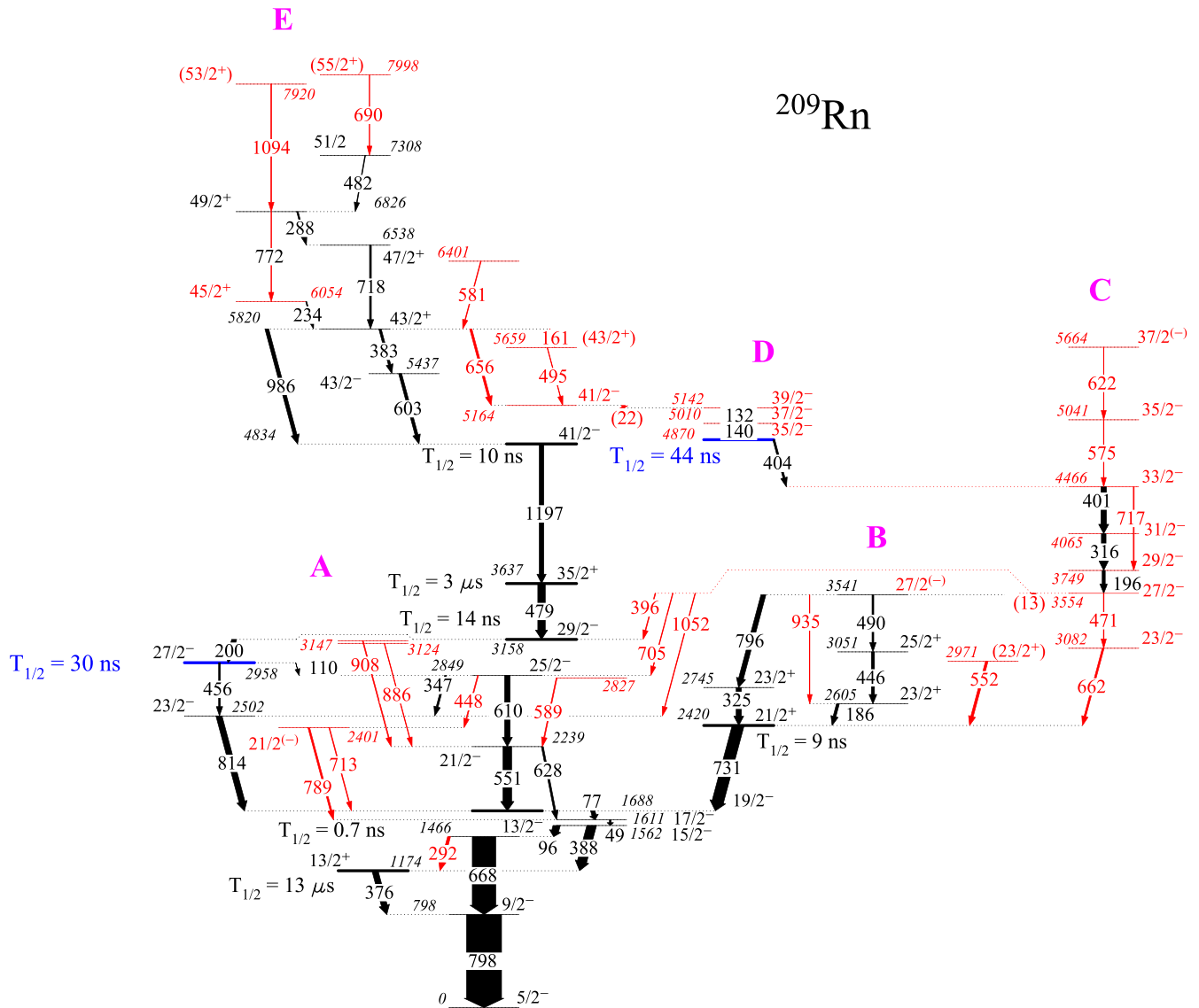


FIG. 1. Proposed level scheme of ^{209}Rn as derived from the present work. The new γ ray transitions, energy levels, and the new assignments of spin-parity, observed in the present work, are indicated in red. The new isomeric state has been indicated in blue.

illustrated in Fig. 1. 26 new γ ray transitions have been placed with the spin-parity assignment of the new levels as well as the already existing levels. The spin-parity assignments of some of the levels have been modified from the earlier work [23] which has been discussed in the following sections. The new γ ray transitions, energy levels, and the assignments of spin-parity, observed in the present work, are indicated in red. Due to the presence of two μs isomeric states with $J^\pi = 13/2^+$ and $35/2^+$ at the excitation energies of 1174 keV and 3637 keV, respectively, the relative intensities of the transitions above these isomeric states have been obtained from the in-beam data collected in singles mode and then have been normalized with the intensity of 798 keV transition decaying from a $9/2^-$ state to the ground state. Similarly, due to the presence of several ns isomers in the level scheme, the relative intensities of the observed γ rays have been measured at the gates of different coincident transitions and finally normalized to the intensity of the 798 keV ground state transition. The R_{DCO}

and Δ_{asym} values of the γ ray transitions as the function of the γ ray energies have been plotted in Figs. 2(a) and 2(b), respectively. In Fig. 2(a), the values of R_{DCO} have been plotted as obtained in a stretched quadrupole gate. In Fig. 2(b), the transitions on the upper side of the dotted line are electric and those in the lower side of the line are magnetic. The intensities and multiplicities of 77 keV, 49 keV, and 96 keV transitions, decaying from $19/2^-$, $17/2^-$, and $15/2^-$ states, respectively, have been adopted from [23]. The information of all the observed γ -ray energies along with their relative intensities, R_{DCO} , and Δ_{asym} values are listed in Table I.

Several new transitions have been observed below the $35/2^+$ isomeric state in the sequence A. Figure 3(a) shows 668 keV gated spectrum where many new transitions along with the earlier reported ones [23] have been observed. For example, three new transitions of 448, 789, and 713 keV transitions have been observed at the gate of 668 keV, as shown in Fig. 3(a). These transitions are also found to be coincident

TABLE I. The γ ray energies (E_γ), their relative intensities (I_γ) have been shown along with the spin-parity of the initial (J_i^π) and final (J_f^π) states and the energy of the initial state (E_i). The measured values of R_{DCO} and Δ_{asym} are also shown along with the proposed multipolarity ($\sigma\lambda$) of the γ rays. R_{DCO} values enlisted in the table are obtained in a stretched quadrupole gate, except as noted.

E_γ (Err)(keV)	E_i (Err)(keV)	I_γ (Err)	R_{DCO} (Err)	Δ_{asym} (Err)	$J_i^\pi \rightarrow J_f^\pi$	$\sigma\lambda$
(12.8) ^a	3553.6(2)				$27/2^- \rightarrow 27/2^{(-)}$	(M1) ^b
(21.8) ^a	5164.1(3)				$41/2^- \rightarrow 39/2^-$	M1 ^b
49.1(1)	1611.1(1)	5 ^c			$17/2^- \rightarrow 15/2^-$	M1(+E2) ^c
76.8(1)	1687.9(2)	12 ^c			$19/2^- \rightarrow 17/2^-$	M1 + E2 ^c
96.0(1)	1562.0(1)	20 ^c			$15/2^- \rightarrow 13/2^-$	M1 + E2 ^c
109.8(2)	2957.9(2)	0.70(9)	0.77(11)		$27/2^- \rightarrow 25/2^-$	M1 + E2
132.2(2)	5142.3(4)	1.80(8)	0.67(6)		$39/2^- \rightarrow 37/2^-$	M1 + E2
139.7(2)	5010.1(3)	2.05(8)	0.75(6)		$37/2^- \rightarrow 35/2^-$	M1 + E2
161.1(3)	5820.3(3)	0.31(8)			$43/2^+ \rightarrow (43/2^+)$	(M1)
185.9(1)	2605.3(2)	7.92(22)	1.93(11) ^d		$23/2^+ \rightarrow 21/2^+$	M1 + E2
195.8(1)	3749.4(2)	8.65(17)	0.71(3)		$29/2^- \rightarrow 27/2^-$	M1 + E2
200.2(1)	3157.8(2)	13.91(33)	0.71(3)		$29/2^- \rightarrow 27/2^-$	M1 + E2
234.0(1)	6054.3(3)	2.99(9)	1.01(12) ^d	-0.12(9)	$45/2^+ \rightarrow 43/2^+$	M1
287.9(1)	6826.2(3)	4.21(25)	0.95(8) ^d	-0.12(8)	$49/2^+ \rightarrow 47/2^+$	M1
291.7(1)	1465.9(1)	8.10(27)	1.13(23) ^d		$13/2^- \rightarrow 13/2^+$	E1 ^e
315.5(1)	4064.9(2)	13.18(46)	0.59(1)	-0.10(3)	$31/2^- \rightarrow 29/2^-$	M1
325.4(1)	2745.1(2)	14.90(54)	0.63(2)	-0.11(6)	$23/2^+ \rightarrow 21/2^+$	M1
347.3(1)	2848.8(2)	5.33(31)	0.71(5)	+0.01(5)	$25/2^- \rightarrow 23/2^-$	M1 + E2 ^e
376.3(1)	1174.2(1)	17.00(72)	1.10(3)	-0.02(5)	$13/2^+ \rightarrow 9/2^-$	M2 ^f
383.4(1)	5820.3(3)	6.79(30)	1.09(11)	-0.09(10)	$43/2^+ \rightarrow 43/2^-$	E1
388.0(1)	1562.0(1)	26.7(12)	0.79(3)	+0.06(11)	$15/2^- \rightarrow 13/2^+$	E1
396.2(1)	3553.6(2)	2.06(22)	0.79(12)	-0.20(10)	$27/2^- \rightarrow 29/2^-$	M1 + E2
401.2(1)	4466.1(2)	15.59(73)	0.56(2)	-0.12(4)	$33/2^- \rightarrow 31/2^-$	M1
404.3(1)	4870.4(2)	5.65(33)	0.55(4)	-0.02(3)	$35/2^- \rightarrow 33/2^-$	M1 + E2 ^f
445.9(1)	3050.9(2)	8.93(20)	0.68(5)	-0.07(6)	$25/2^+ \rightarrow 23/2^+$	M1(+E2)
448.3(1)	2848.8(2)	2.56(21)	1.03(10)		$25/2^- \rightarrow 21/2^{(-)}$	(E2)
456.4(1)	2957.9(2)	4.88(25)	1.08(9)	+0.13(7)	$27/2^- \rightarrow 23/2^-$	E2
471.2(2)	3553.6(2)	1.73(12)			$27/2^- \rightarrow 23/2^-$	E2 ^e
479.3(1)	3637.1(2)	21.20(37)			$35/2^+ \rightarrow 29/2^-$	E3 ^c
482.1(2)	7308.3(3)	1.95(24)	1.15(15) ^d		$51/2 \rightarrow 49/2^+$	(M1)
490.2(1)	3540.8(2)	5.01(17)	1.2(1) ^d	+0.10(6)	$27/2^{(-)} \rightarrow 25/2^+$	(E1)
494.9(2)	5659.1(3)	1.39(14)	0.73(11) ^d		$(43/2^+) \rightarrow 41/2^-$	(E1)
550.8(1)	2238.6(2)	24.70(55)	0.57(2)	-0.07(16)	$21/2^- \rightarrow 19/2^-$	M1(+E2) ^f
551.5(1)	2971.0(2)	6.99(17)	1.54(17) ^d		$(23/2^+) \rightarrow 21/2^+$	(M1 + E2)
575.2(2)	5041.3(3)	1.44(12)	0.78(15)	-0.37(15)	$35/2^- \rightarrow 33/2^-$	M1 + E2
580.8(1)	6401.1(3)	1.80(5)				
588.5(1)	2827.1(2)	2.70(8)				
602.8(1)	5436.8(3)	8.50(22)	0.43(7)	+0.04(5)	$43/2^- \rightarrow 41/2^-$	M1 + E2
610.3(1)	2848.8(2)	15.60(41)	0.93(7)	+0.10(5)	$25/2^- \rightarrow 21/2^-$	E2
622.2(2)	5663.5(4)	1.20(11)	0.58(9)	-0.25(30)	$37/2^{(-)} \rightarrow 35/2^-$	(M1 + E2)
627.5(1)	2238.6(2)	5.50(24)	0.87(8)	+0.08(11)	$21/2^- \rightarrow 17/2^-$	E2 ^f
656.2(1)	5820.3(3)	6.20(19)	0.60(6)	+0.12(8)	$43/2^+ \rightarrow 41/2^-$	E1
661.7(1)	3081.5(2)	5.10(16)	1.07(1) ^d	+0.19(13)	$23/2^- \rightarrow 21/2^+$	E1
667.8(1)	1465.9(1)	67.1(21)	1.01(3)	+0.07(3)	$13/2^- \rightarrow 9/2^-$	E2
690.0(2)	7998.3(4)	0.70(4)	1.39(24) ^d		$(55/2^+) \rightarrow 51/2^+$	(E2)
704.8(1)	3553.6(2)	1.71(15)	0.53(8)	+0.02(10)	$27/2^- \rightarrow 25/2^-$	M1 + E2 ^e
712.6(1)	2400.5(2)	2.11(19)	0.66(10)		$21/2^{(-)} \rightarrow 19/2^-$	(M1 + E2)
716.6(1)	4466.1(2)	2.50(9)			$33/2^- \rightarrow 29/2^-$	E2 ^e
718.0(1)	6538.3(3)	5.04(28)	1.52(15) ^d	+0.14(6)	$47/2^+ \rightarrow 43/2^+$	E2
731.4(1)	2419.5(2)	33.1(12)	0.78(2)	+0.05(3)	$21/2^+ \rightarrow 19/2^-$	E1
772.0(2)	6826.2(3)	1.36(12)	1.64(38) ^d		$49/2^+ \rightarrow 45/2^+$	E2 ^e
789.4(1)	2400.5(2)	4.84(16)	0.94(11)	+0.11(13)	$21/2^{(-)} \rightarrow 17/2^-$	(E2)
795.6(1)	3540.8(2)	13.68(19)	0.98(8)	-0.14(13)	$27/2^{(-)} \rightarrow 23/2^+$	(M2)
798.0(1)	798.0(1)	100	1.01(2)	+0.11(7)	$9/2^- \rightarrow 5/2^-$	E2
813.9(1)	2501.6(2)	16.90(13)	1.00(3)	+0.07(5)	$23/2^- \rightarrow 19/2^-$	E2

TABLE I. (Continued.)

E_γ (Err)(keV)	E_i (Err)(keV)	I_γ (Err)	R_{DCO} (Err)	Δ_{asym} (Err)	$J_i^\pi \rightarrow J_f^\pi$	$\sigma\lambda$
885.8(2)	3124.4(3)	1.55(9)				
908.1(1)	3146.7(2)	2.55(18)				
935.1(2)	3540.8(2)	0.70(10)			$27/2^{(-)} \rightarrow 23/2^+$	($M2$) ^e
986.4(1)	5820.3(3)	10.50(15)	0.51(6)	+0.30(5)	$43/2^+ \rightarrow 41/2^-$	$E1$
1051.7(2)	3553.6(2)	1.67(14)	0.77(17)	+0.19(11)	$27/2^- \rightarrow 23/2^-$	$E2$ ^d
1093.6(1)	7919.8(3)	2.50(5)			$(53/2^+) \rightarrow 49/2^+$	($E2$)
1196.9(1)	4834.0(2)	13.0(64)		+0.07(6)	$41/2^- \rightarrow 35/2^+$	$E3$ ^c

^aNot observed in the present work but its presence is inferred from the observed coincidence relations below and above the levels.

^bNot measured, assigned on the basis of the spin-parity assignments of the initial and final levels, determined from other decaying γ rays.

^cAdopted from the Ref. [23].

^dFrom the stretched dipole gates of 731, 656 and 986 keV as applicable.

^eassigned on the basis of parallel decay paths from the same level.

^fSame is also assigned at Ref. [23].

with 479, 200, 110 keV transitions, but not in coincidence with the 814, 551, 610, and 347 keV transitions. Hence, by checking the coincidence relationships between these γ rays, a level has been placed at 2401 keV which is populated by 448 keV and decays via 789 and 713 keV transitions to the $17/2^-$ and $19/2^-$ spin states, respectively. A spin assignment of $I = 21/2$ and a tentative parity assignment ($-ve$) has been proposed for the level 2401 keV on the basis of R_{DCO} value and the similar decay paths of 551 keV and 628 keV transitions. A new transition has been observed connecting $13/2^-$ and $13/2^+$ states which is not in coincidence with 668 keV but in coincidence with all other transitions above the $13/2^-$ state as is evident from Figs. 3(a) and 3(b). The level structures above the $21/2^+$ and $35/2^+$ isomeric states and the connections observed between different sequence of states are discussed in the following subsections.

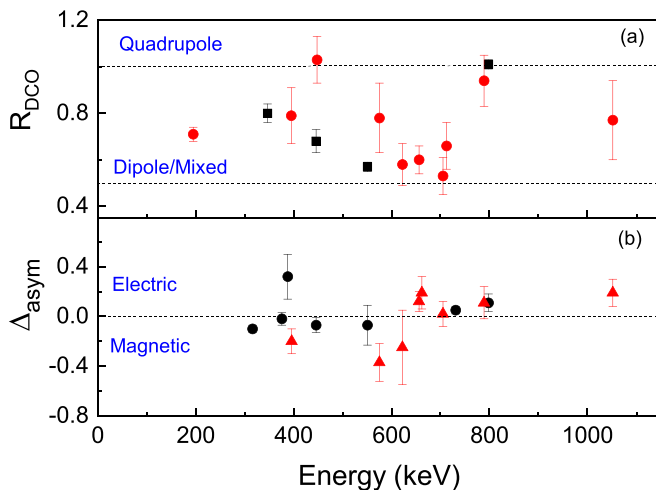


FIG. 2. Plot of (a) R_{DCO} in a quadrupole gate and (b) Δ_{asym} as a function of γ ray energies for the new transitions (in red) and already known transitions (in black). The dotted lines in the y axis in (a) are to guide the eye for the DCO ratio corresponding to pure dipole and quadrupole transitions, respectively. The dotted line in the y axis in (b) is to guide the eye for Δ_{asym} values corresponding to the electric (positive) and magnetic (negative) nature of the transitions.

A. Levels above the $21/2^+$ isomeric state

In the previous work by Poletti *et al.* [23], the spin parities of the levels and the placement of the γ rays feeding the $21/2^+$ state were not confirmed due to the smaller intensities of the various low energy γ rays and the presence of unresolved contaminated peaks. Also, the transitions connecting sequence C with sequences A and E could not be identified. In the present work, six new transitions above this isomeric state have been placed and the spin-parity assignment of the levels above 3541 keV has been modified. The measured Δ_{asym} value of the 490 keV transition from the present work is +0.10(6) which is similar to the Δ_{asym} values of the other stretched electric transitions obtained in the present work. Therefore, along with the DCO ratio measurement, the 490 keV transition has been assigned as $E1$ which corroborates the spin-parity of 3541 keV level as $J^\pi = 27/2^-$. The measured value of Δ_{asym} for 796 keV transition $-0.14(13)$ is also consistent with this result. In the earlier work of Poletti *et al.* [23], on the basis of angular distribution and conversion electron measurement, the 796 keV transition was assigned as $E2$, though, it may have significant contribution from the ground state 798 keV transition. Keeping this in mind and considering the large uncertainty of measured Δ_{asym} , of the 796 keV transition, the parity assignment of 3541 keV level has been made tentative in the present work. Some connecting transitions between sequences A, C and E, D have been observed. A cascade of transitions 471–662 keV has been observed at the coincidence gate of 731 keV transition as shown in Fig. 3(b). These transitions are also found to be in coincidence with all other transitions of the sequences C, D, E but not in coincidence with 796–325 keV and 186–446–490 keV cascade transitions, respectively. Hence these two transitions have been placed in the level scheme, based on their relative intensities, decaying from the levels at 3082 and 3554 keV. The spin-parity of 3082 keV level has been assigned as $23/2^-$ on the basis of R_{DCO} and Δ_{asym} values. But, due to the insufficient counts, the R_{DCO} and Δ_{asym} values of 471 keV transition could not be extracted. On the other hand, several transitions viz. 396, 705, 1052 keV have been observed which connect the 3554 keV level of sequence C with 3158, 2849, and 2502 keV levels of sequence A, respectively. This in turn validates the placement

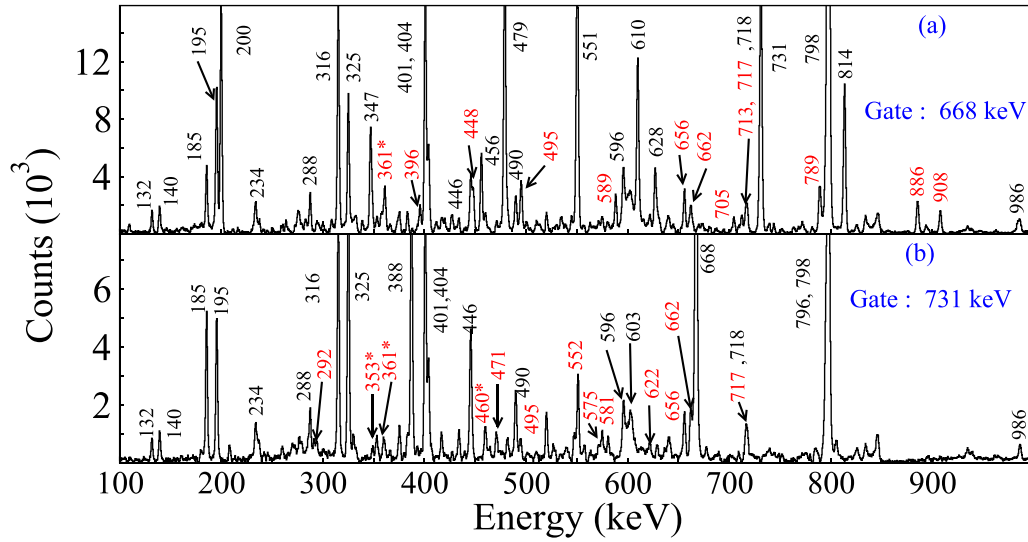


FIG. 3. Coincidence spectra corresponding to the γ ray gates of (a) 668 keV and (b) 731 keV. The new transitions are marked with red, while the transitions marked with an '*' symbol could not be placed in the level scheme.

of the 3554 keV level in the level scheme. The R_{DCO} and Δ_{asym} values of the 396 keV transition (Table I) indicate that this transition to be of $M1 + E2$ nature. The R_{DCO} of the 705 keV transition also supports its dipole assignment. The R_{DCO} of the 1052 keV transition is found to be slightly inconsistent with its quadrupole assignment, which may be due to its weak intensity. However, the Δ_{asym} of the 1052 keV transition supports its electric nature. Thus, the R_{DCO} and Δ_{asym} values of these three transitions together, decaying from the 3554 keV level, suggest that this level can be assigned as $J^\pi = 27/2^-$. This 3554 keV level is connected with the 3541 keV level as all the transitions decaying out from the 3541 keV level are found to be in coincidence with the transitions feeding in the 3554 keV level. This connection of 13 keV (obtained from the difference of the energy levels) has not been observed in the present work but its presence has been inferred on the basis of the coincidence relationships between the γ rays above 3554 keV and below 3541 keV. The γ ray transitions feeding the 3554 keV level in sequences C and D

are also found to be in coincidence with all the transitions below 3158 keV level in sequence A (Fig. 4). Therefore, these three transitions are the connecting transitions between sequences A and C observed in the present work. A cascade of $M1$ transitions, viz. 196, 316, 401, 575, 622, 404, 132, and 140 keV, have been observed above the 3554 keV level which are all in coincidence with the 731 keV transition as illustrated in Fig. 3(b). Most of these transitions are previously known but their placements have been changed from the earlier work depending on the coincidence relationship and the intensity balances. But the two transitions 575 and 622 keV observed in the present work bypass the cascade of the 404, 132, and 140 keV transition and they are not in coincidence with the transitions of sequences D and E.

In the level scheme Fig. 1, the transitions shown in the sequence C forms a cascade of $M1$ transitions. The $M1$ assignments of these transitions have been made on the basis of the R_{DCO} and Δ_{asym} values listed in Table I. Only one crossover $E2$ transition 717 keV has been observed which

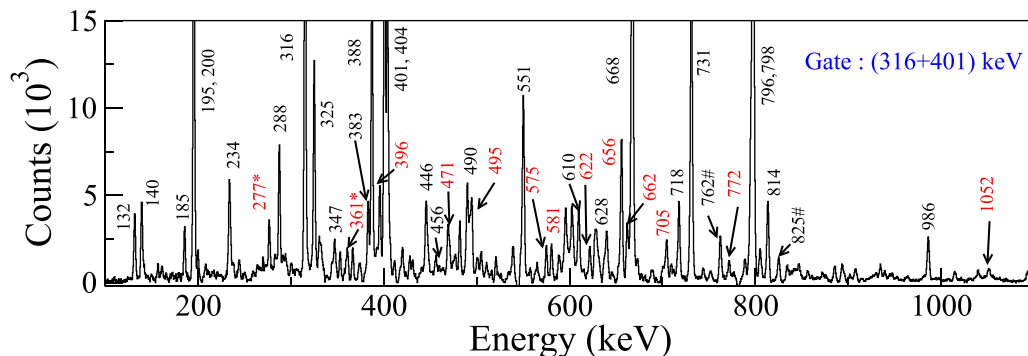


FIG. 4. Coincidence spectrum corresponding to the γ ray gates of 316 and 401 keV. The new transitions are marked with red, while lines from the contaminants are marked with a # symbol and the transitions marked with an '*' symbol could not be placed.

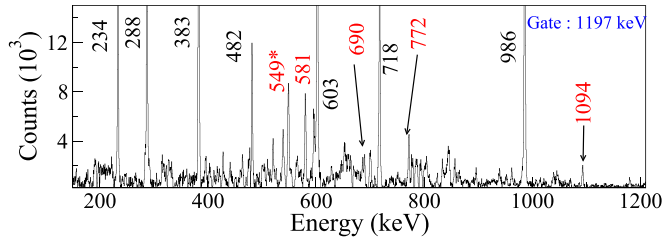


FIG. 5. Coincidence spectrum corresponding to the γ ray gate of 1197 keV. The new transitions are marked with red, while those transitions marked with an * symbol could not be placed.

is not present at the added gate of the 316 and 401 keV transition as shown in Fig. 4. The experimental $B(M1)/B(E2)$ value for this 316-401 keV transition has been determined as $13\mu_N^2/e^2b^2$. This cascade has been interpreted as MR band which is discussed in Sec. VB. So, the sequence of $M1$ γ ray transitions, viz. 196, 316, 401, 404, 132, and 140 keV, above the $27/2^-$ state at 3554 keV level, has been assigned as negative parity sequence in the present work. There is an indication for the possible presence of isomer at $J^\pi = 35/2^-$ state which has been discussed in detail in Sec. IV C.

B. Levels above the $35/2^+$ isomeric state

The placement of 1197 and 479 keV γ ray transitions above and below the $35/2^+$ isomeric state and the $E3$ multipolarity assignments have been adopted from Poletti *et al.* [23]. Figure 5 shows the transitions observed at the gate of the 1197 keV. It has been observed that 718 keV transition is in coincidence with 288 keV but not with 234 keV, rather the 234 and 772 keV transitions are in mutual coincidence with each other. Further, the 482 keV transition has been observed in coincidence with the both 288 and 234 keV γ rays.

Hence, the 772-234 keV cascade has been placed in parallel with the 288-718 keV cascade based on their relative intensities and coincidence relationships. The spin-parity of the level 6054 keV has been obtained from the R_{DCO} and Δ_{asym} values of the 234 keV transition. In addition, two transitions, 690 and 1094 keV, have been observed in sequence E which are placed above the 6826 keV levels based on their coincidence relationships. The transitions feeding the 5820 keV level are found to be in coincidence with all the transitions of sequences C (apart from the 575 and 622 keV γ ray transitions discussed earlier) and D as illustrated in Fig. 6(a). The 656 keV transition is found to be the connecting transition between sequences E, D and E, C. In the earlier work by Poletti *et al.* [23], this 656 keV transition was placed in parallel with the 132 and 796 keV transition. But all the transitions in sequences B, C, and D are found to be in coincidence with the 656 keV transition including 132 and 796 keV. Moreover, all γ rays feeding the 5820 keV level are in coincidence with the 656 keV but the γ rays decaying from this level, viz. 986, 383, 603, 161, and 495 keV transitions, are not observed at the coincidence gate of 656 KeV. The double gated spectrum between the γ rays in sequences D and E, viz., 718 and 404 keV, shows the intensity of 656 keV

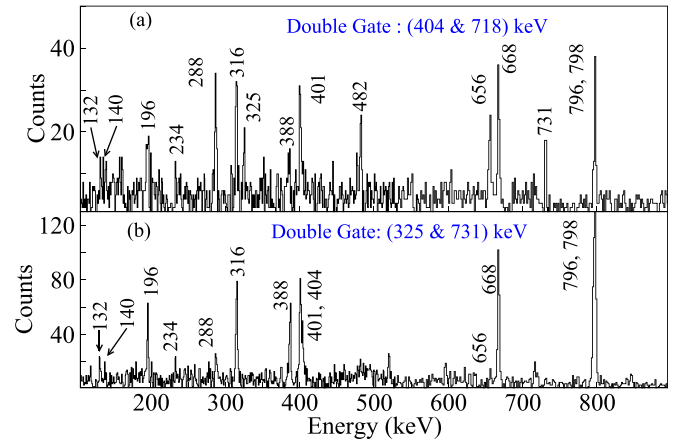


FIG. 6. Double coincidence spectra corresponding to the γ ray gates of (a) 404 and 718 keV, (b) 325 and 731 keV.

transition increases [Fig. 6(a)] compared to the double gated spectrum between the transitions 325 and 731 keV in the same sequence B [Fig. 6(b)]. This strongly suggests the placement of the 656 keV transition as the connecting transition between sequences E and D and nullifies the previous placement of the 656 keV transition [23]. The spin-parity of the 5164 keV level has been determined from the R_{DCO} and Δ_{asym} values of the 656 keV transition. Further, the $E1$ multipolarity of 656 keV derived in the present work validates the spin-parity assignments of both sequences E and D. This 5164 keV level is connected with the 5142 keV level of sequence D as all the transitions decaying out of the 5142 keV level are in coincidence with all the transitions feeding 5164 keV level. This connection of 22 keV (obtained from the difference of energy levels) has not been observed but its presence has been inferred from the observed coincidence relationships. Another cascade of connecting transition 161-495 keV has been observed in parallel with 656 keV although the intensity of this decay path is very weak compared to 656 keV. Due to insufficient statistics, the R_{DCO} and Δ_{asym} of 161 keV transitions could not be determined. For the 495 keV transition, the R_{DCO} could be measured, though with large uncertainties. Also, its R_{DCO} value shows some inconsistency, probably due to its weak nature and difficulties in choosing the suitable gating transition. However, as the spin-parities of the initial level of 161 keV and the final level of 495 keV transitions have already been decided by other parallel decaying γ rays, so the spin-parity of the 5659 keV intermediate level is tentatively assigned as $(43/2^+)$. There is also an indication of the connecting transitions from the 4834 keV level of sequence E to the 4466 keV level of sequence C which are not observed in the present work but can be inferred from the coincidence spectrum of Fig. 4.

C. Possible presence of new isomer

In the present work, the possible presence of an isomeric state at the 4870 keV level has been indicated by the observed intensity difference between the feeding and decaying γ rays of this level. The intensity variation of the transitions above

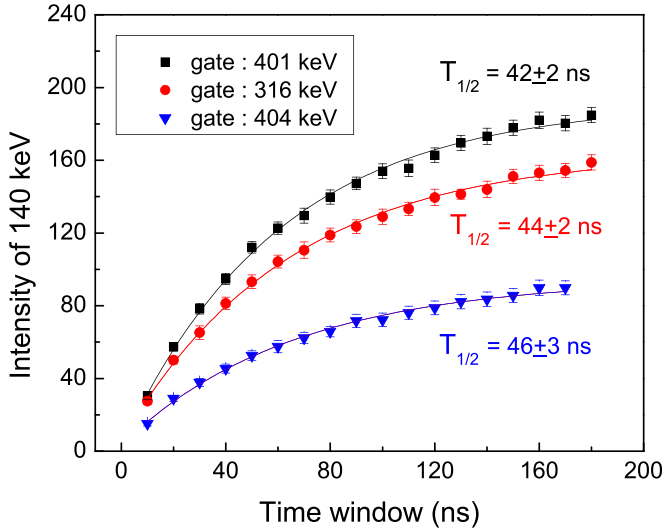


FIG. 7. Intensity variation of 140 keV as a function of the coincidence time window at the gates of 316, 401, 404 keV.

the 4870 keV level, in coincidence with the transitions below this level, were found in two different coincidence time windows of 20 and 200 ns with appropriate normalization. It is observed that there is a significant increase in the intensities of 132 and 140 keV transitions in 200 ns time window, compared to that of 20 ns. This indicates a possible existence of an isomeric state at 4870 keV.

The half-life of the excited state at 4870 keV has been estimated from the variation of the intensity of 140 keV transition (above 4870 keV level) at the coincidence gates of 401, 316, and 404 keV transitions (below 4870 keV level), as a function of different coincident time windows. This intensity variation at different coincidence gates have been fitted by Eq. (4) and are shown in Fig. 7. The half-lives obtained at the three different gating transitions are 44(2), 42(2), and 46(3) ns, respectively. The values obtained from different gates are found to be similar and the half-life of 4870 keV level has been estimated as 44(4) ns. Also, for the level of 2958 keV, there is an intensity difference between the feeding in and decaying out γ rays of the level which indicates possibly another isomeric state exist at that level. The intensity variation of 200 keV γ ray at the gates of 347 and 456 keV has been fitted with Eq. (4) and the half-life ($T_{1/2}$) of the 2958 keV level has been estimated to be 30(2) ns.

V. DISCUSSIONS

The proximity of ^{209}Rn to the doubly magic ^{208}Pb nucleus suggests that the low lying states of ^{209}Rn will be of single particle character. In ^{209}Rn , there are four valence proton particles and three valence neutron holes outside the ^{208}Pb core. Therefore, the excited states in ^{209}Rn can be interpreted by the coupling of odd neutron hole either in $2f_{5/2}$ or in $1i_{13/2}$ orbitals with the even proton core. Proton excitation and neutron excitation to other orbitals becomes important at higher spin.

Computationally, it is highly challenging to perform shell model calculation in the heavy mass region near ^{208}Pb . In the recent years, the extensive shell model calculations have been performed in the region above $Z = 82$ with the availability of modern computational facilities [34–36]. These calculations show reasonable agreement with the experimental results.

The involvement of high- j orbitals for both proton and neutrons also favors shears mechanism to generate magnetic rotational band at high spin. The semiclassical model has been applied for the observed magnetic rotational band in ^{209}Rn , considering a multi-quasiparticle configuration involving valence proton particles and neutron holes in high- j orbitals.

The shell model calculations of low and high spin structures of ^{209}Rn and the semiclassical model calculation for the MR band are discussed in this section.

A. Shell-model calculation

In the present work, shell-model calculations using the KHH7B interaction [37] have been performed. This interaction consists of the four proton orbitals $2d_{5/2}$, $2d_{3/2}$, $3s_{1/2}$, $1h_{11/2}$ below and three orbitals $1h_{9/2}$, $2f_{7/2}$, $1i_{13/2}$ above the $Z = 82$, and four neutron orbitals $2f_{5/2}$, $3p_{3/2}$, $3p_{1/2}$, $1i_{13/2}$ below and three orbitals $2g_{9/2}$, $1i_{11/2}$, $1j_{15/2}$ above $N = 126$. In the KHH7B interaction, the cross shell two-body matrix elements (TBMEs) were generated by the G -matrix potential (H7B) [38], while the proton-neutron, hole-hole, and particle-particle TBMEs are taken from the Kuo-Herling interaction [39] as modified in Ref. [40]. For the present model space to make calculations feasible we have applied truncation. For valence protons, we have completely filled orbitals below $Z = 82$ and allowed four protons to occupy in the $1h_{9/2}$, $2f_{7/2}$, $1i_{13/2}$ orbitals. In the case of valence neutrons, all orbitals below $N = 126$ are open and we allow one neutron excitation across the $N = 126$ shell to occupy in the $2g_{9/2}$ orbital. The shell-model results using this interaction for Rn isotopes for $A = 207$ – 216 are reported in Ref. [34].

The present shell-model results corresponding to the experimental data are shown in Fig. 8 and the configurations of the different states corresponding to the shell-model calculations are shown in Table II.

Up to 1.466 MeV, all the yrast states are in good agreement with the experimental data. The states from $5/2^-$ to $21/2^-$ are assigned with $\pi(h_{9/2}^4) \otimes \nu(f_{5/2}^5 p_{3/2}^4 i_{13/2}^{14})$ configuration. Shell-model reproduces positive as well as negative parity states reasonably well. However, the shell-model results corresponding to the experimentally observed states above 5.66 MeV are much compressed. The compression with the calculated states indicates the need for core-excitation and notable configuration mixing with the higher orbitals beyond $Z = 82$ and $N = 126$ shell closures. Also, the shell model results at the higher spins of sequence C differ from the experimental ones, which suggests a different mechanism of generation of the high angular momentum states, Sec. VB. Experimentally, there are four excited states at 2.4, 3.541, 5.66, and 7.999 MeV with spins $21/2$, $27/2$, $43/2$, and $55/2$, respectively, without any confirmed parity assignments. The shell model calculation suggests that the $21/2$, $27/2$ states

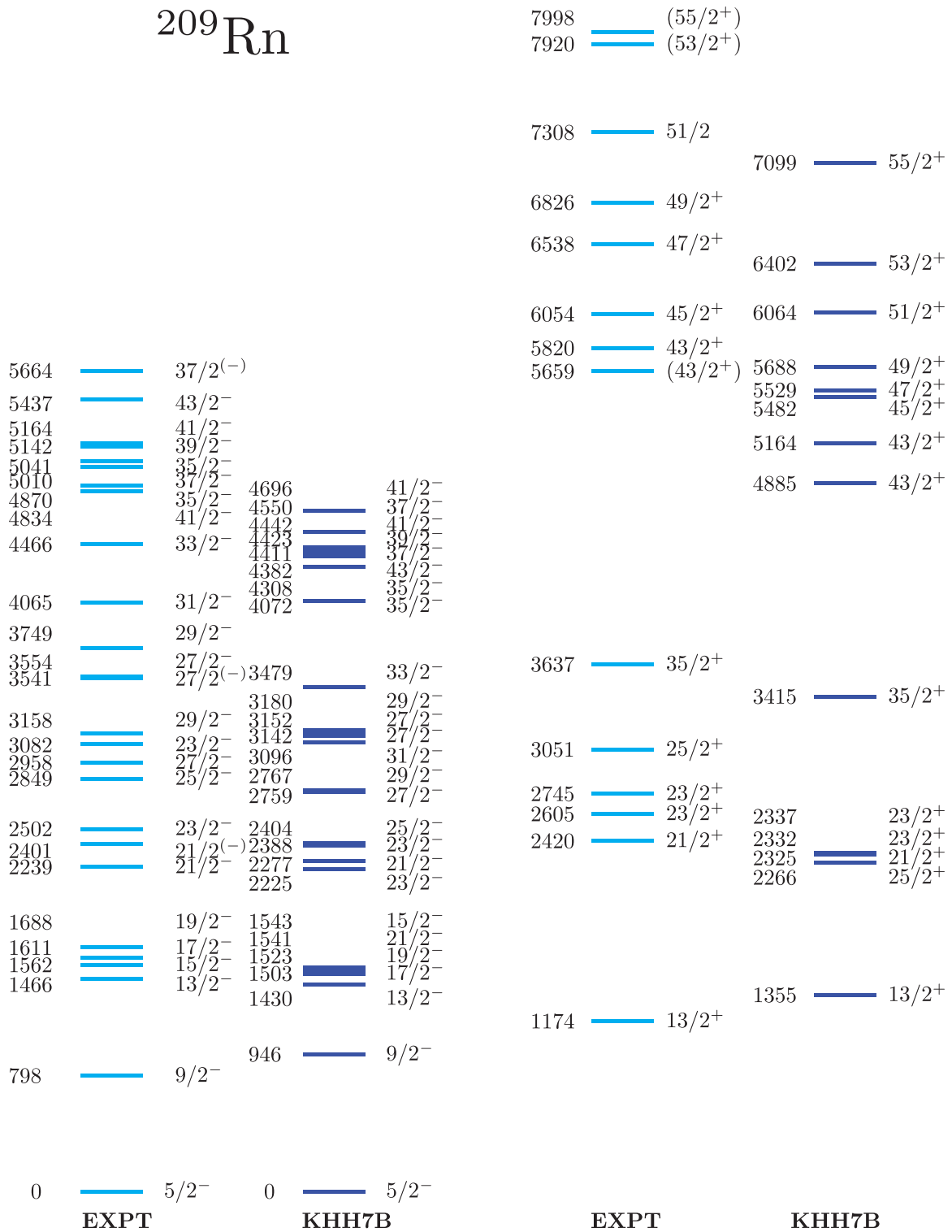


FIG. 8. Comparison of the experimental data with the shell-model using the KHH7B interaction.

will be of negative parity, while $43/2$ and $55/2$ states will be of positive parity.

The half-life ($T_{1/2}$) of the new isomeric state has also been estimated from the shell-model calculation by con-

sidering both the $M1$ and $E2$ transitions from the $35/2^-$ state and the result comes out to be 37.4 ns which is in good agreement with the experimentally measured value of 44(4) ns.

TABLE II. Configurations of different states in ^{209}Rn corresponding to shell-model calculations with the KHH7B interaction. Only the dominant configurations are shown.

State	Configuration	Probability
Negative parity states		
$5/2_1^-$	$\pi(h_{9/2}^4 f_{7/2}^0 i_{13/2}^0) \otimes \nu(f_{5/2}^5 p_{3/2}^4 p_{1/2}^0 i_{13/2}^{14})$	37.70%
$9/2_1^-$	$\pi(h_{9/2}^4 f_{7/2}^0 i_{13/2}^0) \otimes \nu(f_{5/2}^5 p_{3/2}^4 p_{1/2}^0 i_{13/2}^{14})$	23.28%
$13/2_1^-$	$\pi(h_{9/2}^4 f_{7/2}^0 i_{13/2}^0) \otimes \nu(f_{5/2}^5 p_{3/2}^4 p_{1/2}^0 i_{13/2}^{14})$	52.44%
$15/2_1^-$	$\pi(h_{9/2}^4 f_{7/2}^0 i_{13/2}^0) \otimes \nu(f_{5/2}^5 p_{3/2}^4 p_{1/2}^0 i_{13/2}^{14})$	49.18%
$17/2_1^-$	$\pi(h_{9/2}^4 f_{7/2}^0 i_{13/2}^0) \otimes \nu(f_{5/2}^5 p_{3/2}^4 p_{1/2}^0 i_{13/2}^{14})$	51.80%
$19/2_1^-$	$\pi(h_{9/2}^4 f_{7/2}^0 i_{13/2}^0) \otimes \nu(f_{5/2}^5 p_{3/2}^4 p_{1/2}^0 i_{13/2}^{14})$	51.42%
$21/2_1^-$	$\pi(h_{9/2}^4 f_{7/2}^0 i_{13/2}^0) \otimes \nu(f_{5/2}^5 p_{3/2}^4 p_{1/2}^0 i_{13/2}^{14})$	53.88%
$21/2_2^-$	$\pi(h_{9/2}^4 f_{7/2}^0 i_{13/2}^0) \otimes \nu(f_{5/2}^4 p_{3/2}^4 p_{1/2}^1 i_{13/2}^{14})$	40.45%
$23/2_1^-$	$\pi(h_{9/2}^4 f_{7/2}^0 i_{13/2}^0) \otimes \nu(f_{5/2}^4 p_{3/2}^4 p_{1/2}^1 i_{13/2}^{14})$	47.77%
$23/2_2^-$	$\pi(h_{9/2}^4 f_{7/2}^0 i_{13/2}^0) \otimes \nu(f_{5/2}^5 p_{3/2}^4 p_{1/2}^0 i_{13/2}^{14})$	46.48%
$25/2_1^-$	$\pi(h_{9/2}^4 f_{7/2}^0 i_{13/2}^0) \otimes \nu(f_{5/2}^5 p_{3/2}^4 p_{1/2}^0 i_{13/2}^{14})$	54.97%
$27/2_1^-$	$\pi(h_{9/2}^4 f_{7/2}^0 i_{13/2}^0) \otimes \nu(f_{5/2}^5 p_{3/2}^4 p_{1/2}^0 i_{13/2}^{14})$	65.01%
$27/2_2^-$	$\pi(h_{9/2}^3 f_{7/2}^1 i_{13/2}^0) \otimes \nu(f_{5/2}^5 p_{3/2}^4 p_{1/2}^0 i_{13/2}^{14})$	38.57%
$27/2_3^-$	$\pi(h_{9/2}^4 f_{7/2}^0 i_{13/2}^0) \otimes \nu(f_{5/2}^4 p_{3/2}^4 p_{1/2}^1 i_{13/2}^{14})$	45.24%
$29/2_1^-$	$\pi(h_{9/2}^4 f_{7/2}^0 i_{13/2}^0) \otimes \nu(f_{5/2}^5 p_{3/2}^4 p_{1/2}^0 i_{13/2}^{14})$	71.85%
$29/2_2^-$	$\pi(h_{9/2}^3 f_{7/2}^1 i_{13/2}^0) \otimes \nu(f_{5/2}^5 p_{3/2}^4 p_{1/2}^0 i_{13/2}^{14})$	56.78%
$31/2_1^-$	$\pi(h_{9/2}^3 f_{7/2}^1 i_{13/2}^0) \otimes \nu(f_{5/2}^5 p_{3/2}^4 p_{1/2}^0 i_{13/2}^{14})$	50.30%
$33/2_1^-$	$\pi(h_{9/2}^3 f_{7/2}^1 i_{13/2}^0) \otimes \nu(f_{5/2}^5 p_{3/2}^4 p_{1/2}^0 i_{13/2}^{14})$	52.13%
$35/2_1^-$	$\pi(h_{9/2}^3 f_{7/2}^0 i_{13/2}^1) \otimes \nu(f_{5/2}^6 p_{3/2}^4 p_{1/2}^0 i_{13/2}^{13})$	26.42%
$35/2_2^-$	$\pi(h_{9/2}^3 f_{7/2}^0 i_{13/2}^1) \otimes \nu(f_{5/2}^6 p_{3/2}^4 p_{1/2}^0 i_{13/2}^{13})$	33.73%
$37/2_1^-$	$\pi(h_{9/2}^3 f_{7/2}^0 i_{13/2}^1) \otimes \nu(f_{5/2}^5 p_{3/2}^4 p_{1/2}^1 i_{13/2}^{13})$	29.01%
$37/2_2^-$	$\pi(h_{9/2}^3 f_{7/2}^0 i_{13/2}^1) \otimes \nu(f_{5/2}^5 p_{3/2}^4 p_{1/2}^0 i_{13/2}^{14})$	33.59%
$39/2_1^-$	$\pi(h_{9/2}^2 f_{7/2}^2 i_{13/2}^0) \otimes \nu(f_{5/2}^5 p_{3/2}^4 p_{1/2}^0 i_{13/2}^{14})$	37.56%
$41/2_1^-$	$\pi(h_{9/2}^2 f_{7/2}^2 i_{13/2}^0) \otimes \nu(f_{5/2}^5 p_{3/2}^4 p_{1/2}^0 i_{13/2}^{14})$	47.61%
$41/2_2^-$	$\pi(h_{9/2}^3 f_{7/2}^0 i_{13/2}^1) \otimes \nu(f_{5/2}^6 p_{3/2}^4 p_{1/2}^0 i_{13/2}^{13})$	44.99%
$43/2_1^-$	$\pi(h_{9/2}^2 f_{7/2}^2 i_{13/2}^0) \otimes \nu(f_{5/2}^5 p_{3/2}^4 p_{1/2}^0 i_{13/2}^{14})$	40.85%
Positive parity states		
$13/2_1^+$	$\pi(h_{9/2}^4 f_{7/2}^0 i_{13/2}^0) \otimes \nu(f_{5/2}^6 p_{3/2}^4 p_{1/2}^0 i_{13/2}^{13})$	25.52%
$21/2_1^+$	$\pi(h_{9/2}^3 f_{7/2}^1 i_{13/2}^0) \otimes \nu(f_{5/2}^5 p_{3/2}^4 p_{1/2}^0 i_{13/2}^{14})$	40.18%
$23/2_1^+$	$\pi(h_{9/2}^3 f_{7/2}^1 i_{13/2}^0) \otimes \nu(f_{5/2}^5 p_{3/2}^4 p_{1/2}^0 i_{13/2}^{14})$	46.37%
$23/2_2^+$	$\pi(h_{9/2}^3 f_{7/2}^1 i_{13/2}^0) \otimes \nu(f_{5/2}^5 p_{3/2}^4 p_{1/2}^0 i_{13/2}^{14})$	39.38%
$25/2_1^+$	$\pi(h_{9/2}^3 f_{7/2}^1 i_{13/2}^0) \otimes \nu(f_{5/2}^5 p_{3/2}^4 p_{1/2}^0 i_{13/2}^{14})$	46.36%
$35/2_1^+$	$\pi(h_{9/2}^3 f_{7/2}^1 i_{13/2}^0) \otimes \nu(f_{5/2}^5 p_{3/2}^4 p_{1/2}^0 i_{13/2}^{14})$	57.11%
$43/2_1^+$	$\pi(h_{9/2}^3 f_{7/2}^1 i_{13/2}^0) \otimes \nu(f_{5/2}^4 p_{3/2}^4 p_{1/2}^1 i_{13/2}^{14})$	81.21%
$43/2_2^+$	$\pi(h_{9/2}^3 f_{7/2}^1 i_{13/2}^0) \otimes \nu(f_{5/2}^5 p_{3/2}^4 p_{1/2}^0 i_{13/2}^{14})$	58.01%
$45/2_1^+$	$\pi(h_{9/2}^2 f_{7/2}^2 i_{13/2}^0) \otimes \nu(f_{5/2}^6 p_{3/2}^4 p_{1/2}^0 i_{13/2}^{13})$	36.35%

TABLE II. (Continued.)

State	Configuration	Probability
Positive parity states		
$47/2_1^+$	$\pi(h_{9/2}^2 f_{7/2}^2 i_{13/2}^0) \otimes \nu(f_{5/2}^6 p_{3/2}^4 p_{1/2}^0 i_{13/2}^{13})$	38.66%
$49/2_1^+$	$\pi(h_{9/2}^2 f_{7/2}^2 i_{13/2}^0) \otimes \nu(f_{5/2}^6 p_{3/2}^4 p_{1/2}^0 i_{13/2}^{13})$	41.14%
$51/2_1^+$	$\pi(h_{9/2}^2 f_{7/2}^2 i_{13/2}^0) \otimes \nu(f_{5/2}^6 p_{3/2}^4 p_{1/2}^0 i_{13/2}^{13})$	37.60%
$53/2_1^+$	$\pi(h_{9/2}^2 f_{7/2}^2 i_{13/2}^0) \otimes \nu(f_{5/2}^6 p_{3/2}^4 p_{1/2}^0 i_{13/2}^{13})$	43.69%
$55/2_1^+$	$\pi(h_{9/2}^2 f_{7/2}^2 i_{13/2}^0) \otimes \nu(f_{5/2}^5 p_{3/2}^4 p_{1/2}^1 i_{13/2}^{13})$	79.83%

B. Semiclassical model (SCM) calculations for the sequence C

As mentioned earlier in Sec. IV A that a cascade of $M1$ transitions and the regular pattern of the states have been observed above the $27/2\hbar$ state at 3554 keV and up to the $37/2\hbar$ state at 5664 keV. The MR nature of this band has been investigated in the framework of the semiclassical model to extract the information about the effective interaction between the nucleons involved in the shears mechanism. In this model, shears angle θ between the proton angular momentum vector j_π and the neutron angular momentum vector j_ν is derived using the equation

$$\cos \theta = \frac{I(I+1) - j_\pi(j_\pi+1) - j_\nu(j_\nu+1)}{2\sqrt{j_\pi(j_\pi+1)j_\nu(j_\nu+1)}}, \quad (5)$$

where I is the total angular momentum defined as $I = I_{\text{shears}} + R_{\text{core}} \cdot I_{\text{shears}}$ and R_{core} represent the contribution of the angular momentum due to the shears mechanism and the core rotation, respectively. The two spin vectors j_π and j_ν are obtained from the proposed particle-hole configuration. For the observed $M1$ band of sequence C, the proposed particle hole configuration is $[\pi(h_{9/2})^4 \otimes \nu(f_{5/2})^{-2}(p_{1/2})^{-1}]$ with proton angular momentum $j_\pi = 12\hbar$ and neutron angular momentum $j_\nu = 4.5\hbar$. This configuration is in well agreement with the configuration of $J^\pi = 27/2^-$ state at 3554 keV, assigned from the large basis shell-model calculation. The minimum spin I_{min} and the maximum spin I_{max} for this configuration have been calculated as $13.5\hbar$ and $18.5\hbar$, respectively. $I_{\text{min}}(I_{\text{max}})$ corresponds to the band-head spin (termination of the band). The effective interaction between the proton and the neutron blades of the shears band can be written as

$$V(I(\theta)) = E(I) - E_0 = \frac{3}{2}V_2 \cos^2(\theta), \quad (6)$$

where E_0 is the band-head energy, $E(I)$ is the energy of the excited level with the spin (I). V_2 is the second order term of the multipole expansion of effective interaction ($V[I(\theta)]$).

Figure 9 shows the variation of the effective interaction ($V[I(\theta)]$) as a function of the shears angle θ considering the above configuration. The experimental data points are fitted with Eq. (6) which is shown by a red solid line. The value of the interaction strength V_2 between the proton and neutron shears blades is ≈ 1.9 MeV which is found to be in good agreement with the values estimated from the $1/A$ scaling of the corresponding values of $A \approx 200$ reported in this region [11].

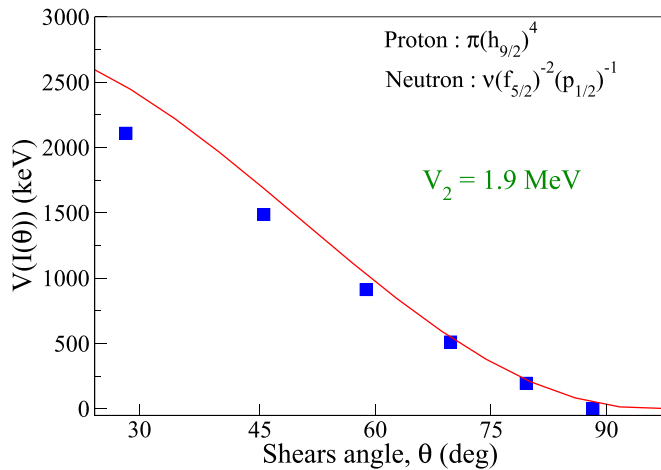


FIG. 9. Variation of the effective interaction as the function of shears angle.

VI. SUMMARY

The high-spin structure of ^{209}Rn has been investigated and a modified level scheme of ^{209}Rn has been proposed in the present work. The connecting transitions between the different

sequence of states have been observed. The possible presence of a new high-spin isomeric state has been indicated. A large basis shell-model calculation with KHH7B interaction has been performed which well reproduces the single-particle excited states. The estimated value of $T_{1/2}$ from shell-model calculation matches well with the experimentally obtained value of the new isomeric state. Further nucleon excitation across $N = 126$ shell is needed to get shell-model results close to the experimental data. A MR band structure has been observed for the first time in ^{209}Rn which has been interpreted under the framework of the semiclassical model (SCM) calculation.

ACKNOWLEDGMENTS

The authors thank the staff of Pelletron Accelerator facility at IUAC for providing the beam. The authors are thankful to Dr. Chandrani Majumder and Mr. Shabir Dar for fruitful discussions on SCM calculation and data analysis procedure. S.D. acknowledges the financial support received from Council of Scientific and Industrial Research (CSIR), India [under File No. 09/667(0001)/2019-EMR-I]. P.C.S. acknowledges a research grant from SERB (India), No. CRG/2022/005167. S.C. is thankful to SERB, India for financial support under N-PDF scheme via Reference No. PDF/2022/001829.

-
- [1] J. B. McGrory and T. T. S. Kuo, *Nucl. Phys. A* **247**, 283 (1975).
 [2] E. Caurier, M. Rejmund, and H. Grawe, *Phys. Rev. C* **67**, 054310 (2003).
 [3] A. K. Jain *et al.*, *Nucl. Data Sheet* **128**, 1 (2015).
 [4] K. Hauschild *et al.*, *Phys. Rev. C* **77**, 047305 (2008).
 [5] A. Gorgen *et al.*, *Nucl. Phys. A* **683**, 108 (2001).
 [6] H. Pai *et al.*, *Phys. Rev. C* **90**, 064314 (2014).
 [7] R. B. Firestone, *Table of Isotopes*, 8th ed. (John Wiley and Sons Inc., 1999).
 [8] A. O. Macchiavelli, R. M. Clark, P. Fallon *et al.*, *Phys. Rev. C* **57**, R1073 (1998).
 [9] A. O. Macchiavelli, R. M. Clark, M. A. Deleplanque, R. M. Diamond, P. Fallon, I. Y. Lee, F. S. Stephens, and K. Vetter, *Phys. Rev. C* **58**, R621 (1998).
 [10] A. O. Macchiavelli, R. M. Clark, M. A. Deleplanque, R. M. Diamond, P. Fallon, I. Y. Lee, F. S. Stephens, and K. Vetter, *Phys. Rev. C* **58**, 3746 (1998).
 [11] R. M. Clark and A. O. Macchiavelli, *Ann. Rev. Nucl. Part. Sci.* **50**, 1 (2000).
 [12] K. Auranen *et al.*, *Phys. Rev. C* **97**, 024301 (2018).
 [13] D. Kanjilal *et al.*, *Eur. Phys. J. A* **58**, 159 (2022).
 [14] R. M. Clark *et al.*, *J. Phys. G* **19**, L57 (1993).
 [15] G. Baldsiefen *et al.*, *Nucl. Phys. A* **592**, 365 (1995).
 [16] D. J. Hartley *et al.*, *Phys. Rev. C* **78**, 054319 (2008).
 [17] J. R. Novak *et al.*, *Phys. Rev. C* **59**, R2989 (1999).
 [18] L. Wan-Ju *et al.*, *Chin. Phys. Lett.* **20**, 632 (2003).
 [19] A. R. Poletti *et al.*, *Nucl. Phys. A* **359**, 180 (1981).
 [20] D. G. Raich *et al.*, *Z. Phys. A: At. Nucl.* **279**, 301 (1976).
 [21] S. Xu *et al.*, *Z. Phys. A: At. Nucl.* **354**, 343 (1996).
 [22] P. Kuusiniemi *et al.*, *Eur. Phys. J. A* **30**, 551 (2006).
 [23] A. R. Poletti *et al.*, *Nucl. Phys. A* **440**, 118 (1985).
 [24] G. K. Mehta and A. P. Patro, *Nucl. Instrum. Meth. Phys. Res. A* **268**, 334 (1988).
 [25] S. Muralithar *et al.*, *Nucl. Instrum. Methods Phys. Res. A* **622**, 281 (2010).
 [26] B. P. Ajith-Kumar *et al.*, in *Proceedings of the DAE Symposium of Nuclear Physics* (Bhabha Atomic Research Centre (BARC), India, 2001), Vol. 44B, p. 390.
 [27] LINUX advanced multiparameter system.
 [28] R. Bhowmik *et al.*, *Proceedings of the DAE Symposium of Nuclear Physics* (Bhabha Atomic Research Centre (BARC), India, 2001), Vol. 44B, p. 422.
 [29] D. C. Radford, *Nucl. Instrum. Methods Phys. Res. A* **361**, 297 (1995).
 [30] A. Kramer-Flecken, T. Morek, R. Lieder *et al.*, *Nucl. Instrum. Methods Phys. Res. A* **275**, 333 (1989).
 [31] G. Duchene *et al.*, *Nucl. Instrum. Methods Phys. Res. A* **432**, 90 (1999).
 [32] K. Starosta *et al.*, *Nucl. Instrum. Methods Phys. Res. A* **423**, 16 (1999).
 [33] S. Chakraborty *et al.*, *Phys. Rev. C* **97**, 054311 (2018).
 [34] B. Bhoj and P. C. Srivastava, *J. Phys. G: Nucl. Part. Phys.* **48**, 125103 (2021).
 [35] K. Yadav *et al.*, *Phys. Rev. C* **107**, 054303 (2023).
 [36] S. Chatterjee *et al.*, *Phys. Rev. C* **106**, 044329 (2022).
 [37] N. A. F. M. Poppelier and P. W. M. Glaudemans, *Z. Phys. A* **329**, 275 (1988).
 [38] A. Hosaka, K.-I. Kubo, and H. Toki, *Nucl. Phys. A* **444**, 76 (1985).
 [39] T. T. S. Kuo and G. Herling, Technical Report No. 2258 (US Naval Research Laboratory, 1971).
 [40] E. K. Warburton and B. A. Brown, *Phys. Rev. C* **43**, 602 (1991).